ELSEVIER

Comput. Methods Appl. Mech. Engrg. 190 (2000) 1163–1185

Computer methods in applied mechanics and engineering

www.elsevier.com/locate/cma

A co-rotational formulation for thin-walled beams with monosymmetric open section

Kuo Mo Hsiao *, Wen Yi Lin

Department of Mechanical Engineering, National Chiao Tung University, 1001 TA Hsueh Road, Hsinchu, Taiwan, ROC

Received 25 August 1999

Abstract

A consistent co-rotational total Lagrangian finite element formulation and numerical procedure for the geometric nonlinear buckling and postbuckling analysis of thin-walled beams with monosymmetric open section is presented. The element developed here has two nodes with seven degrees of freedom per node. The element nodes are chosen to be located at the shear centers of the end cross-sections of the beam element and the shear center axis is chosen to be the reference axis. The deformations of the beam element are described in the current element coordinate system, which is constructed at the current configuration of the beam element. In element nodal forces, all coupling among bending, twisting, and stretching deformations of the beam element is considered by consistent second-order linearization of the fully geometrically nonlinear beam theory. However, the third-order term of the twist rate of the beam axis is considered in element nodal forces. An incremental-iterative method based on the Newton–Raphson method combined with constant arc length of incremental displacement vector is employed for the solution of nonlinear equilibrium equations. The zero value of the tangent stiffness matrix determinant of the structure is used as the criterion of the buckling state. A parabolic interpolation method of the arc length is used to find the buckling load. Numerical examples are presented to demonstrate the accuracy and efficiency of the proposed method.

Keywords: Co-rotational formulation; Thin-walled beam; Geometric nonlinearity; Buckling

1. Introduction

The buckling and postbuckling analyses of thin-walled beams with open section have been the subject of considerable research [1–30]. The buckling of the beam structures is caused by the coupling among bending, twisting, and stretching deformations of the beam members. Thus the buckling analysis is a subtopic of nonlinear rather than linear mechanics [7]. Many different formulations and numerical procedures for the buckling and postbuckling analyses of thin-walled beams have been proposed. Currently, the most popular approach for the analyses of three-dimensional beam is to develop finite element models. The formulations, which have been used in the literature, might be divided into three categories: total Lagrangian (TL) formulation [13–15,17,18,22,25,29], updated Lagrangian (UL) formulation [17,20,28], and co-rotational (CR) formulation [19,21,24,26–28,30]. It is well known that within the co-rotating system either a TL or a UL formulation may be employed [21,31]. These formulations are consequently termed CR–TL and CR–UL formulations. The reference configuration used in a CR–TL formulation differs from the one used in a conventional TL formulation by the motion performed by the co-rotating coordinate system from the initial to the current (or neighboring) configuration. In order to correctly capture all coupling among bending, twisting, and stretching deformations of the beam elements, the formulation of beam elements

* Corresponding author. Fax: +886-35-720-634.
E-mail address: kmhsiao@cc.nctu.edu.tw (K.K. Hsiao).

0045-7825/00/$ - see front matter
PII: S0045-7825(99)00471-5

might be derived by the fully geometrically nonlinear beam theory [32]. The exact expressions for the element nodal forces, which are required in a TL formulation for large rotation/small strain problems, are highly nonlinear functions of element nodal parameters. However, the dominant factors in the geometrical nonlinearities of beam structures are attributable to finite rotations, the strains remaining small. For a beam structure discretized by finite elements, this implies that the motion of the individual elements to a large extent will consist of rigid body motion. If the rigid body motion part is eliminated from the total displacements and the element size is properly chosen, the deformational part of the motion is always small relative to the local element axes; thus in conjunction with the co-rotational formulation, the higher-order terms of nodal parameters in the element nodal forces may be neglected by consistent linearization [21,32]. The so-called 'Natural approach' by Argyris and co-workers, for instance [9–12], was also based on the idea of separating rigid body motions from local deformations.

Hsiao [21] presented a co-rotational total Lagrangian formulation of beam element for the nonlinear analysis of three-dimensional beam structures with large rotations but small strains. Element deformations and element equations were defined in terms of element coordinates, which were constructed at the current configuration of the beam element. The element deformations were determined by the rotation of element cross-section coordinates, which were rigidly tied to element cross-section, relative to the element coordinate system. The beam element developed had two nodes with six degrees of freedom per node. The out-of-plane warping of the cross-section was assumed to be the product of the twist rate of the beam element and the Saint Venant warping function for a prismatic beam of the same cross-section, and the twist rate was assumed to be uniform. In order to correctly capture all coupling among bending, twisting, and stretching deformations of the beam elements, the formulation of beam element was derived by consistent second-order linearization of the fully geometrically nonlinear beam theory. This element was proven to be very effective for geometric nonlinear analysis of three-dimensional beams by numerical examples studied in [21]. The effect of warping restraint is slight and may be negligible in solid sections [33]. Thus, the assumption of uniform twist rate used in [21] may be still appropriate for solid sections with warping restraint. However, the effect of warping restraint is of practical importance in thin-walled sections [33]. Thus, when the restraint of warping is considered, the assumption of uniform twist rate used in [21] is not appropriate for thin-walled sections. When the restraint of warping is considered, the twist rate and the corresponding warping displacement are not uniform for thin-walled open-section beams. The warping bending stress caused by the nonuniform warping displacement could be of the same order of magnitude as the bending stress caused by the applied load for the majority of thin-walled open-section beams. The strain energy corresponding to the warping stress and the associated strain may be equal to the work done by the bimoment [33] upon the twist rate. In [34], the bimoment was considered to be a generalized nodal force and the twist rate to be the associated generalized nodal displacement, and the formulation of the element in [21] was extended to the doubly symmetric thin-walled open-section beams. The beam element proposed in [34] had two nodes with seven degrees of freedom per node. In [21,34], the unit extension of the centroidal axis of the beam element was assumed to be uniform. This assumption might be reasonable for beams with doubly symmetric cross-section, whose centroid and shear center are coincident, because the value of the longitudinal normal strain at the centroid of the cross-section relevant to curvature of the centroidal axis and twist about the shear center axis is zero. However, the assumption of uniform unit extension for centroidal axis may not be applied to thin-walled beams with monosymmetric cross-section, whose shear center and centroid are not coincident, because the longitudinal normal strain at the centroid relevant to the twist about the shear center axis is not equal to zero or uniform. Thus, the kinematics of the element employed in [34] cannot be used to the thin-walled beams with monosymmetric open section. To the authors' knowledge, the application of co-rotational total Lagrangian formulation in the geometric nonlinear buckling and postbuckling analysis for thin-walled beams with monosymmetric open section has not been reported in the literature. The object of this paper is to present a co-rotational total Lagrangian finite element formulation for the geometric nonlinear buckling and postbuckling analysis of thin-walled beams with monosymmetric open section.

Here, the uniform unit extension assumption for centroidal axis used in [34] is modified as that when the longitudinal normal strain at the centroidal axis relevant to the twist about the shear center axis is excluded, the unit extension of the centroid axis of the beam element corresponding to the rest of longitudinal normal

strain is uniform in this study. Following [34], the shear center axis is chosen to be the reference axis and the element nodes are chosen to be located at the shear centers of the end cross-sections of the beam element.

The third-order terms of the nodal parameters are not considered for the element nodal forces in [21]. Timoshenko [35] and Gregory [1] mentioned that owing to this axial deformation, there is an additional resistance of the shaft to torsion proportional to the cube of the twist rate. In the case of a very narrow rectangular cross-section and comparatively large twist rate, the additional resistance corresponding to the cube of the twist rate may contribute an important portion of the total torque [1,30,35]. The values of twist rate, the rate of twist rate and curvature of the beam axis of the beam axis are deformation dependent, not element size dependent. Thus their values may not always be much smaller than unity. It seems that some third-order terms of the element nodal forces, which are relevant to the twist rate, the rate of twist rate and curvature of the beam axis, may not be negligible for some cross-sections with large rotations. In [30,34], it was reported that the third-order term of twist rate was the dominant third-order term of element nodal forces and should be retained for the geometric nonlinear analysis of three-dimensional beams with thin-walled open cross-section. Thus, for simplicity, the third-order term of the twist rate is the only third-order term retained in the element nodal forces in this study.

An incremental-iterative method based on the Newton–Raphson method combined with constant arc length of incremental displacement vector is employed for the solution of nonlinear equilibrium equations. The zero value of the tangent stiffness matrix determinant of the structure is used as the criterion of the buckling state, and the corresponding load is the so-called buckling load. The parabolic interpolation method of the arc length proposed in [34] is employed to find the buckling load. An inverse power method for the solution of the generalized eigenvalue problem is used to find the corresponding buckling mode. In order to initiate the secondary path, at the bifurcation point a perturbation displacement proportional to the first buckling mode is added [36]. Numerical examples are presented to demonstrate the accuracy and efficiency of the proposed method.

2. Finite element formulation

2.1. Basic assumptions

The following assumptions are made in the derivation of behavior of the thin-walled beam element with monosymmetric open section.

1. The beam is prismatic and slender, and the Euler–Bernoulli hypothesis is valid.
2. When the longitudinal normal strain at the centroidal axis relevant to the twist about the shear center axis is excluded, the unit extension of the centroid axis of the beam element corresponding to the rest of longitudinal normal strain is uniform.
3. The cross-section of the beam element does not deform in its own plane and strains within this cross-section can be neglected.
4. The out-of-plane warping of the cross-section is the product of the twist rate of the beam element and the Saint Venant warping function for a prismatic thin walled beam of the same cross-section.
5. The deformation displacements of the beam element are small.
6. The material is homogeneous, isotropic and linear elastic.

In this study, Prandtl's membrane analogy and the Saint Venant torsion theory [29,30,33] are used to obtain an approximate Saint Venant warping function for a prismatic thin-walled beam.

2.2. Coordinate systems

In this paper, a co-rotational total Lagrangian formulation is adopted. In order to describe the system, we define four sets of right-handed rectangular Cartesian coordinate systems:

1. *A fixed global set of coordinates.* X_i^G $(i = 1, 2, 3)$ (see Fig. 1); the nodal coordinates, nodal displacements and rotations, and the stiffness matrix of the system are defined in this coordinates.
2. *Element cross-section coordinates.* x_i^S $(i = 1, 2, 3)$ (see Fig. 1); a set of element cross-section coordinates is associated with each cross-section of the beam element. The origin of this coordinate system is rigidly

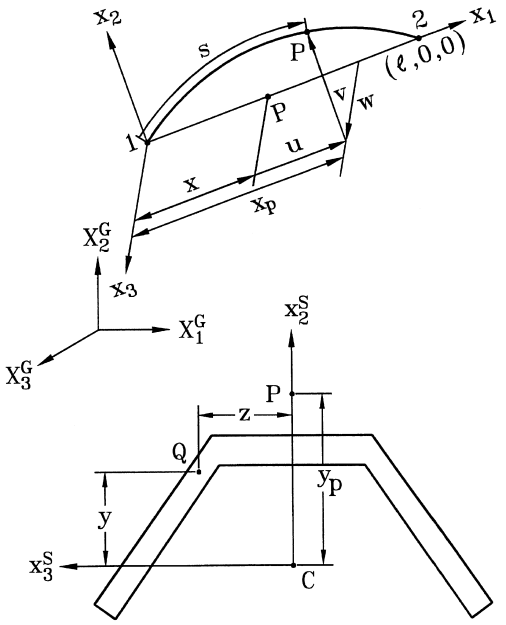

Fig. 1. Coordinate systems.

tied to the *centroid* of the cross-section. The x_1^S axis is chosen to coincide with the *normal of the unwarped* cross-section and the x_2^S and x_3^S axes are chosen to be the *principal centroidal axes* of the cross-section.

3. *Element coordinates*. x_i $(i = 1, 2, 3)$ (see Fig. 1), a set of element coordinates is associated with each element, which is constructed at the current configuration of the beam element. The origin of this coordinate system is located at node 1, and the x_1 axis is chosen to pass through two end nodes (*shear centers of end sections*) of the element; the directions of the x_2 and x_3 axes are chosen to coincide with the direction of the principal centroidal axes of the cross-section in the undeformed state. *Note that this coordinate system is a local coordinate system not a moving coordinate system.* The deformations, internal nodal forces and stiffness matrix of the elements are defined in terms of these coordinates. In this paper, the element deformations are determined by the rotation of element cross-section coordinate systems relative to this coordinate system.
4. *Load base coordinates*. X_i^P $(i = 1, 2, 3)$; a set of load base coordinates is associated with each configuration-dependent moment. The origin of this coordinate system is chosen to be the node where the configuration-dependent moment is applied. The mechanism for generating configuration-dependent moment is described in these coordinates, and the corresponding external load and load stiffness matrix are defined in terms of these coordinates.

In this paper, the symbol { } denotes column matrix. The relations among the global coordinates, element cross-section coordinates, element coordinates and load base coordinates may be expressed by

$$\mathbf{X}^G = \mathbf{A}_{GS}\mathbf{x}^S, \quad \mathbf{X}^G = \mathbf{A}_{GE}\mathbf{x}, \quad \mathbf{X}^G = \mathbf{A}_{GP}\mathbf{X}^P, \tag{1}$$

where $\mathbf{X}^G = \{X_1^G, X_2^G, X_3^G\}$, $\mathbf{x}^S = \{x_1^S, x_2^S, x_3^S\}$, $\mathbf{x} = \{x_1, x_2, x_3\}$, and $\mathbf{X}^P = \{X_1^P, X_2^P, X_3^P\}$; $\mathbf{A}_{GS}$, $\mathbf{A}_{GE}$, and $\mathbf{A}_{GP}$ are matrices of direction cosines of the element cross-section coordinate system, element coordinate system, and load base coordinate system, respectively.

2.3. Rotation vector

For convenience of later discussion, the term 'rotation vector' is used to represent a finite rotation. Fig. 2 shows a vector $\mathbf{b}$ which as a result of the application of a rotation vector $\phi\mathbf{a}$ is transported to the new position $\bar{\mathbf{b}}$. The relation between $\bar{\mathbf{b}}$ and $\mathbf{b}$ may be expressed as [37]:

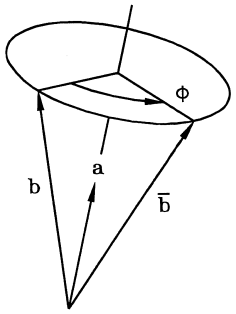

Fig. 2. Rotation vector.

$$\bar{\mathbf{b}} = \cos\phi\mathbf{b} + (1 - \cos\phi)(\mathbf{a}\cdot\mathbf{b})\mathbf{a} + \sin\phi(\mathbf{a}\times\mathbf{b}), \tag{2}$$

where ϕ is the angle of rotation about the axis of rotation, and $\mathbf{a}$ is the unit vector along the axis of rotation.

2.4. Kinematics of beam element

The deformations of the beam element are described in the current element coordinate system. From the kinematic assumptions made in this paper, the deformations of the beam element may be determined by the displacements of the shear center axis of the beam element, orientation of the cross-section (element cross-section coordinates) and the out-of-plane warping of the cross-section. In general, the shear center and centroid are not coincident for thin-walled beams with monosymmetric cross-section. Here, the shear center axis is chosen to be the reference axis and the element nodes are chosen to be located at the shear centers of the end cross-sections of the beam element. Let Q (Fig. 1) be an arbitrary point in the beam element, and P be the point corresponding to Q on the shear center axis. The position vector of point Q in the undeformed and deformed configurations may be expressed as

$$\mathbf{r}_0 = x\mathbf{e}_1 + (y - y_p)\mathbf{e}_2 + z\mathbf{e}_3 \tag{3}$$

and

$$\mathbf{r} = x_p(x)\mathbf{e}_1 + v(x)\mathbf{e}_2 + w(x)\mathbf{e}_3 + \theta_{1,x}\omega\mathbf{e}_1^S + (y - y_p)\mathbf{e}_2^S + z\mathbf{e}_3^S, \tag{4}$$

where y_p is the x_2^S coordinate of point P and y and z are the x_2^S and x_3^Scoordinates of point Q referred to the element cross-section coordinates, respectively, $x_p(x)$, $v(x)$, and $w(x)$ are the x_1, x_2 and x_3 coordinates of point P referred to the current element coordinates, respectively, in the deformed configuration, $\omega = \omega(y,z)$ is the Saint Venant warping function for a prismatic beam of the same cross-section, and $\mathbf{e}_i$ and $\mathbf{e}_i^S$ $(i = 1,2,3)$ denote the unit vectors associated with the x_i and x_i^S axes, respectively. Note that the directions of $\mathbf{e}_i$ and $\mathbf{e}_i^S$ are the same in the undeformed state. Here, the orientations of triad $\mathbf{e}_i^S$ in the deformed state are assumed to be determined by the successive application of the following two rotation vectors to the triad $\mathbf{e}_i$:

$$\boldsymbol{\theta}_n = \theta_n\mathbf{n}, \tag{5}$$

$$\boldsymbol{\theta}_t = \theta_1\mathbf{t}, \tag{6}$$

where

$$\mathbf{n} = \{0,\ \theta_2/(\theta_2^2 + \theta_3^2)^{1/2},\ \theta_3/(\theta_2^2 + \theta_3^2)^{1/2}\}, \tag{7}$$

$$\mathbf{t} = \{\cos\theta_n,\ \theta_3,\ -\theta_2\}, \tag{8}$$

$$\cos\theta_n = (1 - \theta_2^2 - \theta_3^2)^{1/2}, \tag{9}$$

$$\theta_2 = -\frac{\mathrm{d}w(x)}{\mathrm{d}s} = -\frac{\mathrm{d}w(x)}{\mathrm{d}x}\frac{\mathrm{d}x}{\mathrm{d}s} = -\frac{w'}{1+\varepsilon_0}, \qquad \theta_3 = -\frac{\mathrm{d}v(x)}{\mathrm{d}s} = \frac{\mathrm{d}v(x)}{\mathrm{d}x}\frac{\mathrm{d}x}{\mathrm{d}s} = \frac{v'}{1+\varepsilon_0}, \tag{10}$$

$$\varepsilon_0 = \frac{\partial s}{\partial x} - 1 \tag{11}$$

in which $\mathbf{n}$ is the unit vector perpendicular to the vectors $\mathbf{e}_1$ and $\mathbf{e}_1^S$, and $\mathbf{t}$ is the tangent unit vector of the deformed shear center axis of the beam element. Note that the orientation of $\mathbf{e}_1^S$ coincides with that of $\mathbf{t}$. θ_1 is the rotation about vector $\mathbf{t}$. θ_n the angle measured from x_1 axis to vector $\mathbf{t}$, ε_0 the unit extension of the shear center axis and s is the arc length of the deformed shear center axis measured from node 1 to point P. In this paper, the symbol $(\,)'$ denotes $(\,)_{,x} = \partial(\,)/\partial x$.

Using Eqs. (2)–(8), the relation between the vectors $\mathbf{e}_i$ and $\mathbf{e}_i^S$ $(i = 1, 2, 3)$ in the element coordinate system may be obtained as [21]:

$$\mathbf{e}_i^S = \mathbf{R}\mathbf{e}_i, \tag{12}$$

where $\mathbf{R}$ is the so-called rotation matrix. The rotation matrix is determined by θ_i $(i = 1, 2, 3)$. Thus, θ_i are called rotation parameters in this study.

Let $\boldsymbol{\theta} = \{\theta_1, \theta_2, \theta_3\}$ be the column matrix of rotation parameters, $\delta\boldsymbol{\theta}$ be the variation of $\boldsymbol{\theta}$. The triad $\mathbf{e}_i^S$ $(i = 1, 2, 3)$ corresponding to $\boldsymbol{\theta}$ may be rotated by a rotation vector $\delta\boldsymbol{\phi} = \{\delta\phi_1, \delta\phi_2, \delta\phi_3\}$ to reach their new positions corresponding to $\boldsymbol{\theta} + \delta\boldsymbol{\theta}$ [21]. When θ_2 and θ_3 are much smaller than unity, the relationship between $\delta\boldsymbol{\theta}$ and $\delta\boldsymbol{\phi}$ may be approximated by [21]

$$\delta\boldsymbol{\theta} = \begin{bmatrix} 1 & \theta_3/2 & -\theta_2/2 \\ -\theta_3 & 1 & 0 \\ \theta_2 & 0 & 1 \end{bmatrix} \delta\boldsymbol{\phi} = \mathbf{T}^{-1}\delta\boldsymbol{\phi}. \tag{13}$$

The relationship among $x_p(x)$, $v(x)$, $w(x)$ in Eq. (4) may be given as

$$x_p(x) = u_1 + \int_0^x [(1+\varepsilon_0)^2 - v_{,x}^2 - w_{,x}^2]^{1/2}\mathrm{d}x, \tag{14}$$

where u_1 is the displacement of node 1 in the x_1 direction. Note that due to the definition of the element coordinate system, the value of u_1 is equal to zero. However, the variation of u_1 is not zero. Making use of Eq. (14), one obtains

$$\ell = L + u_2 - u_1 = x_p(L) - x_p(0) = \int_0^L [(1+\varepsilon_0)^2 - v_{,x}^2 - w_{,x}^2]^{1/2}\mathrm{d}x \tag{15}$$

in which ℓ is the current chord length of the shear center axis of the beam element, and L the length of the undeformed beam axis, and u_2 is the displacement of node 2 in the x_1 direction.

Here, the lateral deflections of the shear center axis, $v(x)$ and $w(x)$, and the rotation about the shear center axis, $\theta_1(x)$, are assumed to be the Hermitian polynomials of x. $v(x)$, $w(x)$ and $\theta_1(x)$ may be expressed by

$$v(x) = \mathbf{N}_b^t\mathbf{u}_b, \quad w(x) = \mathbf{N}_c^t\mathbf{u}_c, \quad \theta_1(x) = \mathbf{N}_d^t\mathbf{u}_d, \tag{16}$$

$$\mathbf{u}_b = \{v_1, v_1', v_2, v_2'\}, \quad \mathbf{u}_c = \{w_1, -w_1', w_2, -w_2'\}, \quad \mathbf{u}_d = \{\theta_{11}, \beta_1, \theta_{12}, \beta_2\}, \tag{17}$$

where v_j and w_j $(j = 1, 2)$ are nodal values of v and w at nodes j, respectively, v_j' and w_j' $(j = 1, 2)$ are nodal values of $v_{,x}$ and $w_{,x}$ at nodes j, respectively, and θ_{1j} and β_j $(j = 1,\ 2)$ are nodal values of $\theta_1, \theta_{1,x}$ at nodes j, respectively. Note that, due to the definition of the element coordinates, the values of v_j and w_j $(j = 1, 2)$ are zero. However, their variations are not zero.

The axial displacements of the shear center axis may be determined from the lateral deflections and the unit extension of the shear center axis using Eq. (14).

If x, y and z in Eq. (3) are regarded as the Lagrangian coordinates, the Green strain ε_{11}, ε_{12} and ε_{13} are given by [38]:

$$\varepsilon_{11} = \tfrac{1}{2}(\mathbf{r}'_{,x}\mathbf{r}_{,x} - 1), \tag{18a}$$

$$\varepsilon_{12} = \tfrac{1}{2}\mathbf{r}'_{,x}\mathbf{r}_{,y}, \tag{18b}$$

$$\varepsilon_{13} = \tfrac{1}{2}\mathbf{r}'_{,x}\mathbf{r}_{,z}. \tag{18c}$$

Substituting Eqs. (4) and (12) into Eq. (18a) and retaining all terms up to the second-order yields

$$\begin{aligned}\varepsilon_{11} = {} & \varepsilon_0 - (y-y_p)\theta_{3,x} + z\theta_{2,x} + \omega\theta_{1,xx} + \tfrac{1}{2}\varepsilon_0^2 + \omega\varepsilon_0\theta_{1,xx} + (y-y_p)(\theta_1\theta_{2,x} - \varepsilon_0\theta_{3,x}) + z(\theta_1\theta_{3,x} + \varepsilon_0\theta_{2,x}) \\ & - (y-y_p)\omega\theta_{3,x}\theta_{1,xx} + z\omega\theta_{2,x}\theta_{1,xx} + \tfrac{1}{2}(y-y_p)^2(\theta_{1,x}^2 + \theta_{3,x}^2) + \tfrac{1}{2}z^2(\theta_{1,x}^2 + \theta_{2,x}^2) - (y-y_p)z\theta_{2,x}\theta_{3,x} \\ & + \tfrac{1}{2}\omega^2\theta_{1,xx}^2.\end{aligned} \tag{19}$$

When ε_{11} at the centroidal axis ($x = y = 0$) relevant to the twist about the shear center axis is excluded, ε_c, the unit extension of the centroidal axis of the beam element corresponding to the rest of ε_{11} in Eq. (19) may be expressed as

$$\tfrac{1}{2}[(1+\varepsilon_c)^2 - 1] = \varepsilon_0 + y_p\theta_{3,x} - \theta_{2,x} + \tfrac{1}{2}\varepsilon_0^2 + y_p\varepsilon_0\theta_{3,x} + \tfrac{1}{2}y_p^2\theta_{3,x}^2. \tag{20}$$

From Eq. (20), one may obtain

$$\varepsilon_0 = \varepsilon_c - y_p\theta_{3,x}. \tag{21}$$

Substituting Eq. (21) into Eq. (15) and making use of assumption (2), one may obtain ε_c as

$$\varepsilon_c = \frac{\ell - L}{L} + \frac{y_p}{L}(\theta_{32} - \theta_{31}) + \frac{1}{2L}\int_0^L (v_{,x}^2 + w_{,x}^2)\,\mathrm{d}x. \tag{22}$$

Substituting Eq. (21) into Eq. (19), one may obtain

$$\varepsilon_{11} = \varepsilon_{11}^1 + \varepsilon_{11}^2, \tag{23a}$$

$$\varepsilon_{11}^1 = \varepsilon_c - yv_{,xx} - zw_{,xx} + \omega\theta_{1,xx}, \tag{23b}$$

$$\begin{aligned}\varepsilon_{11}^2 = {} & \tfrac{1}{2}\varepsilon_c^2 + \varepsilon_{0,x}(yv_{,x} + zw_{,x}) + \omega\varepsilon_c\theta_{1,xx} + \tfrac{1}{2}[(y-y_p)^2 + z^2]\theta_{1,x}^2 + (\tfrac{1}{2}y^2 - y_py)v_{,xx}^2 + \tfrac{1}{2}z^2w_{,xx}^2 + \tfrac{1}{2}\omega^2\theta_{1,xx}^2 \\ & - (y-y_p)\theta_1w_{,xx} + z\theta_1v_{,xx} + (yz - y_pz)v_{,xx}w_{,xx} - y\omega v_{,xx}\theta_{1,xx} - z\omega w_{,xx}\theta_{1,xx},\end{aligned} \tag{23c}$$

where ε_{11}^k $(k = 1, 2)$ represent the kth-order terms of ε_{11}.

Substituting Eqs. (4) and (12) into Eqs. (18b) and (18c) and retaining all terms up to the second-order yields

$$\varepsilon_{12} = \varepsilon_{12}^1 + \varepsilon_{12}^2, \tag{24a}$$

$$\varepsilon_{12}^1 = \tfrac{1}{2}(\omega_{,y} - z)\theta_{1,x}, \tag{24b}$$

$$\varepsilon_{12}^2 = \tfrac{1}{2}[\omega_{,y}\varepsilon_c\theta_{1,x} + (\omega - y\omega_{,y})\,\theta_{1,x}v_{,xx} - z\omega_{,y}\theta_{1,x}w_{,xx} + \omega\omega_{,y}\theta_{1,x}\theta_{1,xx}] + \tfrac{1}{4}z(v_{,x}w_{,xx} - w_{,x}v_{,xx}), \tag{24c}$$

$$\varepsilon_{13} = \varepsilon_{13}^1 + \varepsilon_{13}^2, \tag{25a}$$

$$\varepsilon_{13}^1 = \tfrac{1}{2}[\omega_{,z} + (y-y_p)]\,\theta_{1,x}, \tag{25b}$$

$$\varepsilon_{13}^2 = \tfrac{1}{2}[\omega_{,z}\varepsilon_c\theta_{1,x} + (\omega - z\omega_{,z})\,\theta_{1,x}w_{,xx} - y\omega_{,z}\theta_{1,x}v_{,xx} + \omega\omega_{,z}\theta_{1,x}\theta_{1,xx}] + \tfrac{1}{4}(y-y_p)(w_{,x}v_{,xx} - v_{,x}w_{,xx}), \tag{25c}$$

where ε_{1j}^k $(j = 2, 3;\ k = 1, 2)$ represent the kth-order terms of ε_{11}.

2.5. Nodal parameters and forces

The element proposed here has two nodes with seven degrees of freedom per node. Two sets of element nodal parameters termed 'explicit nodal parameters' and 'implicit nodal parameters' are employed. The explicit nodal parameters of the element are used for the assembly of the system equations from the element equations. They are chosen to be u_{ij} ($u_{1j}=u_j$, $u_{2j}=v_j$, $u_{3j}=w_j$), the x_i ($i=1,2,3$) components of the translation vectors $\mathbf{u}_j$ at node j ($j=1,2$), ϕ_{ij}, the x_i ($i=1,2,3$) components of the rotation vectors $\boldsymbol{\phi}_j$ at node j ($j=1,2$), and β_j, the twist rate of the shear center axis at node j. Here, the values of $\boldsymbol{\phi}_j$ are reset to zero at current configuration. Thus, $\delta\phi_{ij}$, the variation of ϕ_{ij}, represents infinitesimal rotations about the x_i axes [21], and the generalized nodal forces corresponding to $\delta\phi_{ij}$ are m_{ij}, the conventional moments about the x_i axes. The generalized nodal forces corresponding to δu_{ij}, the variations of u_{ij} are f_{ij}, the forces in the x_i directions. The generalized nodal forces corresponding to $\delta\beta_j$, the variations of β_j, are bimoment B_j.

The implicit nodal parameters of the element are used to determine the deformation of the beam element. They are chosen to be u_{ij}, the x_i ($i=1,2,3$) components of the translation vectors $\mathbf{u}_j$ at node j ($j=1,2$), θ_{1j}, β_j, v'_j, and w'_j ($j=1,2$) defined in Eq. (17). Let θ^*_{1j}, θ^*_{2j} and θ^*_{3j} ($j=1,\ 2$) denote θ_{1j}, $-w'_j$ and v'_j, respectively. The generalized nodal forces corresponding to δu_{ij}, $\delta\theta^*_{1j}$ and $\delta\beta_j$ are f_{ij}, m^θ_{ij} and B_j, the forces in the x_i directions, the generalized moments, and bimoments, respectively. Note that m^θ_{ij} are not conventional moments, because $\delta\theta^*_{1j}$ are not infinitesimal rotations about the x_i axes at deformed state.

In view of Eqs. (10) and (13), the relations between the variation of the implicit and explicit nodal parameters may be expressed as

$$\delta\mathbf{q}_\theta=\begin{Bmatrix}\delta\mathbf{u}_1\\ \delta\boldsymbol{\theta}^*_1\\ \delta\mathbf{u}_2\\ \delta\boldsymbol{\theta}^*_2\\ \delta\boldsymbol{\beta}\end{Bmatrix}=\begin{bmatrix}\mathbf{I}_3 & \mathbf{0} & \mathbf{0} & \mathbf{0} & \bar{\mathbf{0}}\\ \mathbf{T}_{b1} & \mathbf{T}_{a1} & -\mathbf{T}_{b1} & \mathbf{T}_{c1} & \bar{\mathbf{0}}\\ \mathbf{0} & \mathbf{0} & \mathbf{I}_3 & \mathbf{0} & \bar{\mathbf{0}}\\ \mathbf{T}_{b2} & \mathbf{T}_{c2} & -\mathbf{T}_{b2} & \mathbf{T}_{a2} & \bar{\mathbf{0}}\\ \bar{\mathbf{0}}^t & \bar{\mathbf{0}}^t & \bar{\mathbf{0}}^t & \bar{\mathbf{0}}^t & \mathbf{I}_2\end{bmatrix}=\begin{Bmatrix}\delta\mathbf{u}_1\\ \delta\boldsymbol{\phi}_1\\ \delta\mathbf{u}_2\\ \delta\boldsymbol{\phi}_2\\ \delta\boldsymbol{\beta}\end{Bmatrix}=\mathbf{T}_{\theta\phi}\delta\mathbf{q}, \tag{26}$$

$$\mathbf{T}_{aj}=\begin{bmatrix}1 & \theta_{3j}/2 & -(\theta_{2j}/2)\\ -\theta_{3j} & 1+\varepsilon_{0j} & 0\\ \theta_{2j} & 0 & 1+\varepsilon_{0j}\end{bmatrix}+(-1)^j\begin{bmatrix}0 & 0 & 0\\ 0 & 0 & -(3y_p/L)\theta_{2j}\\ 0 & 0 & -(3y_p/L)\theta_{3j}\end{bmatrix},$$

$$\mathbf{T}_{bj}=\begin{bmatrix}0 & 0 & 0\\ -(\theta_{2j}/L) & 0 & 0\\ -(\theta_{3j}/L) & 0 & 0\end{bmatrix}+(-1)^j\begin{bmatrix}0 & 0 & 0\\ 0 & -(6y_p/L^2)\theta_{2j} & 0\\ 0 & -(6y_p/L^2)\theta_{3j} & 0\end{bmatrix}, \tag{27}$$

$$\mathbf{T}_{cj}=(-1)^j\begin{bmatrix}0 & 0 & 0\\ 0 & (3z_p/L)\theta_{2j} & -(3y_p/L)\theta_{2j}\\ 0 & (3z_p/L)\theta_{3j} & -(3y_p/L)\theta_{3j}\end{bmatrix}\quad(j=1,2),$$

where $\delta\mathbf{u}_j=\{\delta u_j,\delta v_j,\delta w_j\}$, $\delta\boldsymbol{\theta}^*_j=\{\delta\theta_{1j},-\delta w'_j,\delta v'_j\}$, $\delta\boldsymbol{\phi}_j=\{\delta\phi_{1j},\delta\phi_{2j},\delta\phi_{3j}\}$ ($j=1,2$) and $\delta\boldsymbol{\beta}=\{\delta\beta_1,\delta\beta_2\}$; $\mathbf{I}_2$ and $\mathbf{I}_3$ are the identity matrices of order 2×2 and 3×3, respectively, $\mathbf{0}$ and $\bar{\mathbf{0}}$ are zero matrices of order 3×3 and 3×2, respectively, and ε_{0j} ($j=1,2$) are the nodal values of ε_0 at node j.

Let $\mathbf{f}=\{\mathbf{f}_1,\mathbf{m}_1,\mathbf{f}_2,\mathbf{m}_2,\mathbf{B}\}$, $\mathbf{f}_\theta=\{\mathbf{f}_1,\mathbf{m}^\theta_1,\mathbf{f}_2,\mathbf{m}^\theta_2\mathbf{B}\}$, where $\mathbf{f}_j=\{f_{1j},f_{2j},f_{3j}\}$, $\mathbf{m}_j=\{m_{1j},m_{2j},m_{3j}\}$, $m^\theta_j=\{m^\theta_{1j},m^\theta_{2j},m^\theta_{3j}\}$ ($j=1,2$), and $\mathbf{B}=\{B_1,B_2\}$, denote the internal nodal force vectors corresponding to the variation of the explicit and implicit nodal parameters, $\delta\mathbf{q}$ and $\delta\mathbf{q}_\theta$, respectively. Using the contragradient law [39] and Eq. (26), the relation between $\mathbf{f}$ and $\mathbf{f}_\theta$, may be given by

$$\mathbf{f}=\mathbf{T}^t_{\theta\phi}\mathbf{f}_\theta. \tag{28}$$

The global nodal parameters for the structural system corresponding to the element local nodes j ($j=1,2$) should be consistent with the element explicit nodal parameters. Thus, they are chosen to be U_{ij}, the X_i ($i=1,2,3$) components of the translation vectors $\mathbf{U}_j$ at node j ($j=1,2$) , Φ_{ij}, the X_i ($i=1,2,3$) components of the rotation vectors $\boldsymbol{\Phi}_j$ at nodes j ($j=1,2$), and β_j, the twist rate of the shear center axis at node j. Here, the values of $\boldsymbol{\Phi}_j$ are reset to zero at current configuration. Thus, $\delta\Phi_{ij}$, the variations of Φ_{ij},

represent infinitesimal rotations about the X_i axes [21], and the generalized nodal forces corresponding to $\delta\Phi_{ij}$ are the conventional moments about the X_i axes. The generalized nodal forces corresponding to δU_{ij}, the variation of U_{ij} are the forces in the X_i directions. The generalized nodal forces corresponding to $\delta\beta_j$, the variation of β_j are B_j.

2.6. Element nodal force vector

The element nodal force vector $\mathbf{f}_\theta$ (Eq. (28)) corresponding to the implicit nodal parameters is obtained from the virtual work principle in the current element coordinates. It should be mentioned again that *the element coordinate system is a local coordinate system not a moving coordinate system.* Thus, a standard procedure is used here for the derivation of $\mathbf{f}_\theta$. For convenience, the implicit nodal parameters are divided into four generalized nodal displacement vectors u_i $(i = a, b, c, d)$, where

$$\mathbf{u}_a = \{u_1, u_2\} \tag{29}$$

and $\mathbf{u}_b$, $\mathbf{u}_c$, and $\mathbf{u}_d$ are defined in Eq. (17).

The generalized force vectors corresponding to $\delta\mathbf{u}_i$, the variation of $\mathbf{u}_i$ $(i = a, b, c, d)$, are

$$\begin{aligned} &\mathbf{f}_a = \{f_{11}, f_{12}\}, && \mathbf{f}_b = \{f_{21}, m^\theta_{31}, f_{22}, m^\theta_{32}\},\\ &\mathbf{f}_c = \{f_{31}, m^\theta_{21}, f_{32}, m^\theta_{22}\}, && \mathbf{f}_d = \{m^\theta_{11}, B_1, m^\theta_{12}, B_2\}. \end{aligned} \tag{30}$$

The virtual work principle requires that

$$\delta\mathbf{u}_a^t\mathbf{f}_a + \delta\mathbf{u}_b^t\mathbf{f}_b + \delta\mathbf{u}_c^t\mathbf{f}_c + \delta\mathbf{u}_d^t\mathbf{f}_d = \int_V (\sigma_{11}\delta\varepsilon_{11} + 2\sigma_{12}\delta\varepsilon_{12} + 2\sigma_{13}\delta\varepsilon_{13})\,\mathrm{d}V, \tag{31}$$

where V is the volume of the undeformed beam, $\delta\varepsilon_{1j}$ $(j = 1, 2, 3)$ are the variations of ε_{1j} in Eqs. (23a)–(25c) respectively, with respect to the implicit nodal parameter. σ_{1j} $(j = 1, 2, 3)$ are the second Piola–Kirchhoff stresses. For linear elastic material, the following constitutive equations are used:

$$\sigma_{11} = E\varepsilon_{11}, \quad \sigma_{12} = 2G\varepsilon_{12} \quad \text{and} \quad \sigma_{13} = 2G\varepsilon_{13} \tag{32}$$

in which E is Young's modulus and G is the shear modulus.

If the element size is chosen to be sufficiently small, the values of the rotation parameters of the deformed element defined in the current element coordinate system may always be much smaller than unity. Thus the higher-order terms of rotation parameters in the element internal nodal forces may be neglected. However, in order to include the nonlinear coupling among the bending, twisting, and stretching deformations, the terms up to the second-order of rotation parameters and their spatial derivatives are retained in element internal nodal forces by consistent second-order linearization of Eq. (31). However, the values of $\theta_{1,x}$, $\theta_{1,xx}$, $v_{,xx}$ and $w_{,xx}$ in Eqs. (23a)–(25c) are deformation dependent, not element size dependent. Thus their values may not always be much smaller than unity and their third-order terms may not be negligible. In [30,34], it was reported that the third-order term of twist rate is the dominant third-order term of element nodal forces and should be retained for the geometric nonlinear analysis of three-dimensional beams with thin walled open cross-section. Thus, for simplicity, the third-order term of the twist rate $\theta_{1,x}$ is the only third-order term retained in the element nodal forces in this study.From Eqs. (23a)–(25c),(29)–(32) we may obtain

$$\mathbf{f}_a = [A_1 - AE\varepsilon_c(y_p\mathbf{B}^t\mathbf{u}_b)]\mathbf{G}_a, \tag{33}$$

$$\begin{aligned} \mathbf{f}_b = {} & EI_z(1+\varepsilon_c)\int \mathbf{N}''_b v_{,xx}\,\mathrm{d}x + \frac{y_p}{L}A_1\mathbf{B} + y_pEI_y\int \mathbf{N}'''_b w_{,x}w_{,xx}\,\mathrm{d}x + y_pEI_z\int \mathbf{N}'''_b v_{,x}v_{,xx}\,\mathrm{d}x + f_{12}L\mathbf{G}_b\\ & - EI_z\int \varepsilon_{0,x}(\mathbf{N}'_b v_{,xx} + \mathbf{N}''_b v_{,x})\,\mathrm{d}x + E(I_z - I_y)\int \mathbf{N}''_b\theta_1 w_{,xx}\,\mathrm{d}x + \left[GJ_z - \frac{E}{2}(\alpha_z + \alpha_{yz} - 2y_pI_z)\right]\\ & \times \int \mathbf{N}''_b\theta^2_{1,x}\,\mathrm{d}x - E\left(\frac{3}{2}\alpha_z - 3y_pI_z\right)\int \mathbf{N}''_b v^2_{,xx}\,\mathrm{d}x - E\left(\frac{3}{2}\alpha_{yz} - y_pI_y\right)\int \mathbf{N}''_b w^2_{,xx}\,\mathrm{d}x\\ & - \frac{3}{2}E\alpha_{\omega z}\int \mathbf{N}''_b\theta^2_{1,xx}\,\mathrm{d}x + 3E\alpha_{\omega yz}\int \mathbf{N}''_b\theta_{1,xx}w_{,xx}\,\mathrm{d}x + \frac{1}{2}GJ\int (\mathbf{N}''_b\theta_{1,x}w_{,x} - \mathbf{N}'_b\theta_{1,x}w_{,xx})\,\mathrm{d}x, \end{aligned} \tag{34}$$

$$\mathbf{f}_c = EI_y(1+\varepsilon_c)\int \mathbf{N}_c'' w_{,xx}\,\mathrm{d}x + f_{12}L\mathbf{G}_c - EI_y\int \varepsilon_{0,x}(\mathbf{N}_c' w_{,xx} + \mathbf{N}_c'' w_{,x})\,\mathrm{d}x + AEy_p\varepsilon_c\int \mathbf{N}_c''\theta_1\,\mathrm{d}x$$
$$+ E(I_z - I_y)\int \mathbf{N}_c''\theta_1 v_{,xx}\,\mathrm{d}x + 3E\alpha_{\omega yz}\int \mathbf{N}_c''\theta_{1,xx}v_{,xx}\,\mathrm{d}x$$
$$- E(3\alpha_{yz} - 2y_pI_y)\int \mathbf{N}_c'' v_{,xx}w_{,xx}\,\mathrm{d}x + \frac{1}{2}GJ\int (\mathbf{N}_c'\theta_{1,x}v_{,xx} - \mathbf{N}_c''\theta_{1,x}v_{,x})\,\mathrm{d}x, \tag{35}$$

$$\mathbf{f}_d = [GJ + (EI_p + AEy_p^2)\varepsilon_c]\int \mathbf{N}_d'\theta_{1,x}\,\mathrm{d}x + EI_\omega(1+3\varepsilon_c)\int \mathbf{N}_d''\theta_{1,xx}\,\mathrm{d}x + AEy_p\varepsilon_c\int \mathbf{N}_d w_{,xx}\,\mathrm{d}x$$
$$- 3E\alpha_{\omega z}\int \mathbf{N}_d''\theta_{1,xx}v_{,xx}\,\mathrm{d}x + 3E\alpha_{\omega yz}\int \mathbf{N}_d'' v_{,xx}w_{,xx}\,\mathrm{d}x + E(I_z - I_y)\int \mathbf{N}_d v_{,xx}w_{,xx}\,\mathrm{d}x$$
$$+ \frac{1}{2}GJ\int \mathbf{N}_d'(w_{,x}v_{,xx} - v_{,x}w_{,xx})\,\mathrm{d}x + [2GJ_z - E(\alpha_z + \alpha_{yz} - 2y_pI_z)]\int \mathbf{N}_d'\theta_{1,x}v_{,xx}\,\mathrm{d}x$$
$$+ \underline{\frac{1}{2}EK_I\int \mathbf{N}_d\theta_{1,x}^3\,\mathrm{d}x}, \tag{36}$$

$$A_1 = AEL\varepsilon_c + \frac{3}{2}AEL\varepsilon_c^2 + \frac{1}{2}(EI_p + AEy_p^2)\int \theta_{1,x}^2\,\mathrm{d}x + \frac{3}{2}EI_\omega\int \theta_{1,xx}^2\,\mathrm{d}x + \frac{1}{2}EI_y\int w_{,xx}^2\,\mathrm{d}x$$
$$+ \frac{1}{2}EI_z\int v_{,xx}^2\,\mathrm{d}x + AEy_p\int \theta_1 w_{,xx}\,\mathrm{d}x, \tag{37}$$

$$\mathbf{B} = \{0,\ -1,\ 0,\ 1\},\quad \mathbf{G}_a = \frac{1}{L}\{-1,\ 1\},\quad \mathbf{G}_b = \frac{1}{L}\int \mathbf{N}_b' v_{,x}\,\mathrm{d}x - \frac{y_p}{L}\varepsilon_c\mathbf{B} + \frac{y_p^2}{L^2}\mathbf{Q}\mathbf{u}_b,$$

$$\mathbf{G}_c = \frac{1}{L}\int \mathbf{N}_c' w_{,x}\,\mathrm{d}x,\quad \mathbf{Q} = L(\mathbf{N}_{b2}'\mathbf{N}_{b2}''' - \mathbf{N}_{b1}'\mathbf{N}_{b1}''' + \mathbf{N}_{b2}'''\mathbf{N}_{b2}'' - \mathbf{N}_{b1}'''\mathbf{N}_{b1}'') - \mathbf{B}\mathbf{B}^t, \tag{38}$$

$$I_y = \int z^2\,\mathrm{d}A,\quad I_z = \int y^2\,\mathrm{d}A,\quad K_I = \int [(y-y_p)^2 + z^2]^2\,\mathrm{d}A,\quad \alpha_z = \int y^3\,\mathrm{d}A,$$

$$\alpha_{yz} = \int z^2 y\,\mathrm{d}A,\quad I_\omega = \int \omega^2\,\mathrm{d}A,\quad \alpha_{\omega z} = \int \omega^2 y\,\mathrm{d}A,\quad \alpha_{\omega yz} = \int \omega yz\,\mathrm{d}A,\quad I_p = I_y + I_z,$$

$$J = \int \{(-z + \omega_{,y})^2 + [(y-y_p) + \omega_{,z}]^2\}\,\mathrm{d}A,$$

$$J_z = \int [z(y\omega_{,y} - \omega) - y(y-y_p)\omega_{,z} - y(\omega_{,y}^2 + \omega_{,z}^2) + \omega\omega_{,y}]\,\mathrm{d}A, \tag{39}$$

in which the range of integration for the integral $\int(\ )\,\mathrm{d}x$ in Eqs. (34)–(38) is from 0 to L, A is the cross-section area, $\mathbf{N}_k$ $(k = b, c, d)$ are given in Eq. (17), and $\mathbf{N}_{kj}$ are nodal values of $\mathbf{N}_k$ at nodes j $(j = 1, 2)$. The underlined term in Eq. (36) is the third-order term of $\theta_{1,x}$.

The element nodal force vector $\mathbf{f}$ (Eq. (28)) corresponding to the explicit nodal parameters may be obtained from Eqs. (28) and (33)–(36). Note that only the terms up to the second-order of nodal parameters and the third-order terms of $\theta_{1,x}$, are retained in $\mathbf{f}_\theta$. Thus, the corresponding $\mathbf{f}$ in Eq. (28) may be rewritten as

$$\mathbf{f} = \mathbf{f}_\theta + (\mathbf{T}_{\theta\phi}^t - \mathbf{I}_{14})\mathbf{f}_\theta^1, \tag{40}$$

where $\mathbf{f}_\theta^1$ is the first-order terms of nodal parameters of $\mathbf{f}_\theta$, and $\mathbf{I}_{14}$ is the identity matrix of order 14×14.

2.7. Element tangent stiffness matrices

The element tangent stiffness matrix corresponding to the explicit nodal parameters (referred to as explicit tangent stiffness matrix) may be obtained by differentiating the element nodal force vector $\mathbf{f}$ in Eq. (40) with respect to explicit nodal parameters. Using Eqs. (26) and (40), we obtain

$$\mathbf{k} = \frac{\partial \mathbf{f}}{\partial \mathbf{q}} = \frac{\partial \mathbf{f}}{\partial \mathbf{q}_\theta}\frac{\partial \mathbf{q}_\theta}{\partial \mathbf{q}} = [\mathbf{k}_\theta + (\mathbf{T}'_{\theta\phi} - \mathbf{I}_{14})\mathbf{k}^0_\theta + \mathbf{H}]\mathbf{T}_{\theta\phi}, \tag{41}$$

where $\mathbf{k}_\theta = \partial \mathbf{f}_\theta / \partial \mathbf{q}_\theta$ is the tangent stiffness matrix corresponding to implicit nodal parameters (referred to as implicit tangent stiffness matrix), $\mathbf{k}^0_\theta$ the zeroth-order terms of nodal parameters of $\mathbf{k}_\theta$, and $\mathbf{H}$ is an unsymmetrical matrix and is given by

$$\mathbf{H} = \begin{bmatrix} \mathbf{0} & \mathbf{h}_{b1} & \mathbf{0} & \mathbf{h}_{b2} & \bar{\mathbf{0}} \\ \mathbf{h}^t_{b1} & \mathbf{h}_{a1} & -\mathbf{h}^t_{b1} & \mathbf{h}_c & \bar{\mathbf{0}} \\ \mathbf{0} & -\mathbf{h}_{b1} & \mathbf{0} & -\mathbf{h}_{b2} & \bar{\mathbf{0}} \\ \mathbf{h}^t_{b2} & \mathbf{h}^t_c & -\mathbf{h}^t_{b2} & \mathbf{h}_{a2} & \bar{\mathbf{0}} \\ \bar{\mathbf{0}}^t & \bar{\mathbf{0}}^t & \bar{\mathbf{0}}^t & \bar{\mathbf{0}}^t & \mathbf{0}_2 \end{bmatrix}, \tag{42}$$

$$\mathbf{h}_{aj} = \begin{bmatrix} 0 & m^{\theta 1}_{3j} & -m^{\theta 1}_{2j} \\ 0 & 0 & (1/2)m^{\theta 1}_{1j} \\ 0 & -(1/2)m^{\theta 1}_{1j} & 0 \end{bmatrix} + (-1)^j \begin{bmatrix} 0 & 0 & 0 \\ 0 & 0 & -(3y_p/L)m^{\theta 1}_{2j} \\ 0 & -(3y_p/L)m^{\theta 1}_{2j} & -(6y_p/L)m^{\theta 1}_{3j} \end{bmatrix},$$

$$\mathbf{h}_{bj} = \begin{bmatrix} 0 & -(1/L)m^{\theta 1}_{2j} & -(1/L)m^{\theta 1}_{3j} \\ 0 & 0 & 0 \\ 0 & 0 & 0 \end{bmatrix} + (-1)^j \begin{bmatrix} 0 & 0 & 0 \\ 0 & -(6y_p/L^2)m^{\theta 1}_{2j} & -(6y_p/L^2)m^{\theta 1}_{3j} \\ 0 & 0 & 0 \end{bmatrix} \quad (j = 1, 2),$$

$$\mathbf{h}_c = \begin{bmatrix} 0 & 0 & 0 \\ 0 & 0 & (3y_p/L)m^{\theta 1}_{21} \\ 0 & -(3y_p/L)m^{\theta 1}_{22} & (3y_p/L)(m^{\theta 1}_{31} - m^{\theta 1}_{32}) \end{bmatrix}, \tag{43}$$

where $\mathbf{0}_2$, $\mathbf{0}$ and $\bar{\mathbf{0}}$ are zero matrices of order 2×2, 3×3 and 3×2, respectively; $m^{\theta 1}_{ij}$ $(i = 1, 2, 3,\ j = 1, 2)$ are the first-order terms of m^θ_{ij}.

Note that the element tangent stiffness matrix in Eq. (41) is asymmetric. However, the structural tangent stiffness matrix becomes symmetric at equilibrium configuration [19,27,40].

Using the direct stiffness method, the implicit tangent stiffness matrix $\mathbf{k}_\theta$ may be assembled by the submatrices

$$\mathbf{k}_{ij} = \frac{\partial \mathbf{f}_i}{\partial \mathbf{u}_j}, \tag{44}$$

where $\mathbf{f}_i$ $(i = a, b, c, d)$ are defined in Eqs. (33)–(36) and $\mathbf{u}_i$ $(i = a, b, c, d)$ are defined in Eqs. (17) and (29). Note that $\mathbf{k}_{ij}$ are symmetric matrices. The explicit form of $\mathbf{k}_{ij}$ may be expressed as

$$\mathbf{k}_{aa} = AEL\left(1 + 3\varepsilon_c - 2\frac{y_p}{L}\mathbf{B}^t\mathbf{u}_b\right)\mathbf{G}_a\mathbf{G}^t_a,$$

$$\mathbf{k}_{ab} = \mathbf{G}_a\left[AEL\mathbf{G}_b^t + AEy_p\left(1+2\varepsilon_c - \frac{y_p}{L}\mathbf{B}^t\mathbf{u}_b\right)\mathbf{B}^t + EI_z\int \mathbf{N}_b'''^t v_{,xx}\,\mathrm{d}x\right],$$

$$\mathbf{k}_{ac} = \mathbf{G}_a\left(AEL\mathbf{G}_c^t + AEy_p\int \mathbf{N}_c'''^t\theta_1\,\mathrm{d}x + EI_y\int \mathbf{N}_c'''^t w_{,xx}\,\mathrm{d}x\right),$$

$$\mathbf{k}_{ad} = \mathbf{G}_a\left[(EI_p + AEy_p^2)\int \mathbf{N}_d'''^t\theta_{1,x}\,\mathrm{d}x + AEy_p\int \mathbf{N}_d''^t w_{,xx}\,\mathrm{d}x + 3EI_\omega\int \mathbf{N}_d'''^t\theta_{1,xx}\,\mathrm{d}x\right],$$

$$\begin{aligned}\mathbf{k}_{bb} = {} & EI_z(1+\varepsilon_c)\int \mathbf{N}_b''\mathbf{N}_b''\,\mathrm{d}x + \frac{AEy_p^2}{L}[(1+2\varepsilon_c)\mathbf{B}\mathbf{B}^t + \varepsilon_c\mathbf{Q}] + AEy_p(\mathbf{G}_b\mathbf{B}^t + \mathbf{B}\mathbf{G}_b^t)\\ & - EI_z\varepsilon_{0,x}\int(\mathbf{N}_b'\mathbf{N}_b'''^t + \mathbf{N}_b''\mathbf{N}_b''^t)\,\mathrm{d}x + f_{12}\int \mathbf{N}_b'\mathbf{N}_b''^t\,\mathrm{d}x - 3E(\alpha_z - 2y_pI_z)\int \mathbf{N}_b''\mathbf{N}_b'''^t v_{,xx}\,\mathrm{d}x\\ & + y_pEI_z\int\left[\left(\mathbf{N}_b'''\mathbf{N}_b''^t + \mathbf{N}_b'\mathbf{N}_b'''^t + \frac{1}{L}\mathbf{N}_b''\mathbf{B}^t + \frac{1}{L}\mathbf{B}\mathbf{N}_b'''^t\right)v_{,xx} + (\mathbf{N}_b'''\mathbf{N}_b''^t + \mathbf{N}_b''\mathbf{N}_b'''^t)v_{,x}\right]\mathrm{d}x,\end{aligned}$$

$$\begin{aligned}\mathbf{k}_{bc} = {} & AEy_p\mathbf{B}\mathbf{G}_c^t + \frac{AEy_p^2}{L}\int \mathbf{B}\mathbf{N}_c'''^t\theta_1\,\mathrm{d}x + E(I_z - I_y)\int \mathbf{N}_b''\mathbf{N}_c'''^t\theta_1\,\mathrm{d}x\\ & + y_pEI_y\int\left[\left(\mathbf{N}_b'''\mathbf{N}_c''^t + \frac{1}{L}\mathbf{B}\mathbf{N}_c'''^t\right)w_{,xx} + \mathbf{N}_b'''\mathbf{N}_c'''^t w_{,x}\right]\mathrm{d}x + 3E\alpha_{\omega yz}\int \mathbf{N}_b''\mathbf{N}_c'''^t\theta_{1,xx}\,\mathrm{d}x\\ & - E(3\alpha_{yz} - 2y_pI_y)\int \mathbf{N}_b''\mathbf{N}_c''w_{,xx}\,\mathrm{d}x + \frac{1}{2}GJ\int(\mathbf{N}_b''\mathbf{N}_c''^t - \mathbf{N}_b'\mathbf{N}_c''')\theta_{1,x}\,\mathrm{d}x,\end{aligned}$$

$$\begin{aligned}\mathbf{k}_{bd} = {} & \frac{y_p}{L}(EI_p + AEy_p^2)\int \mathbf{B}\mathbf{N}_d'^t\theta_{1,x}\,\mathrm{d}x + \frac{3y_pEI_\omega}{L}\int \mathbf{B}\mathbf{N}_d'''^t\theta_{1,xx}\,\mathrm{d}x + \frac{AEy_p^2}{L}\int \mathbf{B}\mathbf{N}_d^t w_{,xx}\,\mathrm{d}x\\ & - 3E\alpha_{\omega z}\int \mathbf{N}_b''\mathbf{N}_d'''^t\theta_{1,xx}\,\mathrm{d}x + 3E\alpha_{\omega yz}\int \mathbf{N}_b''\mathbf{N}_d'''^t w_{,xx}\,\mathrm{d}x + E(I_z - I_y)\int \mathbf{N}_b''\mathbf{N}_d^t w_{,xx}\,\mathrm{d}x\\ & + \frac{1}{2}GJ\int(\mathbf{N}_b''\mathbf{N}_d'^t w_{,x} - \mathbf{N}_b'\mathbf{N}_d'^t w_{,xx})\,\mathrm{d}x + [2GJ_z - E(\alpha_z + \alpha_{yz} - 2y_pI_z)]\int \mathbf{N}_b''\mathbf{N}_d'^t\theta_{1,x}\,\mathrm{d}x,\end{aligned}$$

$$\begin{aligned}\mathbf{k}_{cc} = {} & EI_y(1+\varepsilon_c)\int \mathbf{N}_c''\mathbf{N}_c'''^t\,\mathrm{d}x - EI_y\varepsilon_{0,x}\int(\mathbf{N}_c'\mathbf{N}_c'''^t + \mathbf{N}_c''\mathbf{N}_c''^t)\,\mathrm{d}x + f_{12}\int \mathbf{N}_c'\mathbf{N}_c''^t\,\mathrm{d}x\\ & - E(3\alpha_{yz} - 2y_pI_y)\int \mathbf{N}_c''\mathbf{N}_c'''^t v_{,xx}\,\mathrm{d}x,\end{aligned}$$

$$\begin{aligned}\mathbf{k}_{cd} = {} & AEy_p\varepsilon_c\int \mathbf{N}_c''\mathbf{N}_d^t\,\mathrm{d}x + 3E\alpha_{\omega yz}\int \mathbf{N}_c''\mathbf{N}_d'''^t v_{,xx}\,\mathrm{d}x + E(I_z - I_y)\int \mathbf{N}_c''\mathbf{N}_d^t v_{,xx}\,\mathrm{d}x\\ & + \frac{1}{2}GJ\int(\mathbf{N}_c'\mathbf{N}_d''^t v_{,xx} - \mathbf{N}_c''\mathbf{N}_d'^t v_{,x})\,\mathrm{d}x,\end{aligned}$$

$$\begin{aligned}\mathbf{k}_{dd} = {} & [GJ + (EI_p + AEy_p^2)\varepsilon_c]\int \mathbf{N}_d'\mathbf{N}_d'^t\,\mathrm{d}x + EI_\omega(1+3\varepsilon_c)\int \mathbf{N}_d''\mathbf{N}_d'''^t\,\mathrm{d}x - 3E\alpha_{\omega z}\int \mathbf{N}_d''\mathbf{N}_d'''^t v_{,xx}\,\mathrm{d}x\\ & + [2GJ_z - E(\alpha_z + \alpha_{yz} - 2y_pI_z)]\int \mathbf{N}_d'\mathbf{N}_d''^t v_{,xx}\,\mathrm{d}x + \underline{\frac{3}{2}EK_I\int \mathbf{N}_d'\mathbf{N}_d''^t\theta_{1,x}^2\,\mathrm{d}x},\end{aligned} \tag{45}$$

where the underlined term is the second-order term of $\theta_{1,x}$.

The element tangent stiffness matrix referred to the global coordinate system is obtained by using the standard coordinate transformation.

2.8. Load stiffness matrix

Different ways for generating configuration-dependent moment were proposed in the literature [8,11,27]. Here, for simplicity, only the conservative moments generated by conservative force or forces (with fixed directions) are considered, and one of the ways for generating conservative moment proposed in [27] is employed here. For completeness, a brief description of the way for generating conservative moment is given here. In this study, a set of load base coordinates X_i^P $(i = 1, 2, 3)$ associated with each configuration-dependent moment is constructed at the current configuration. The mechanism for generating configuration-dependent moment is described in these coordinates, and the corresponding external load and load stiffness matrix [41] are defined in terms of these coordinates. Unless stated otherwise, all vectors and matrices in this section are referred to these coordinates. Note that this coordinate system is just a local coordinate system constructed at the current configuration, not a moving coordinate system. Thus, it is regarded as a fixed coordinate system in the derivation of the load stiffness matrix.

The way for generating configuration-dependent moment may described as follows.

Consider a rigid arm of length R whose end is rigidly connected with the structure at node O as shown in Fig. 3. The other end of the rigid arm is acted upon by a conservative force (with a fixed direction) of magnitude P. The origin of the load base coordinates X_i^P $(i = 1, 2, 3)$ is chosen to be located at the node O. The X_1^P axis is chosen to coincide with the axis of the rigid arm, and the X_2^P and X_3^P axes are perpendicular to the rigid arm.

The external moment vector at node O generated by the above mentioned mechanism may be expressed by

$$\mathbf{M} = RP\mathbf{t}^P \times \mathbf{e}_p^P, \tag{46}$$

where $\mathbf{e}_p^P = \{\ell_1, \ell_2, \ell_3\}$ is the unit vector in the direction of $\mathbf{P}$, and $\mathbf{t}^P$ is the unit vector in the axial direction of the rigid arm. Note that $\mathbf{t}^P$ coincides with $\mathbf{e}_1^P = \{1, 0, 0\}$, the unit vector associated with the X_1^P axis. The corresponding load stiffness matrix may be expressed as

$$\mathbf{k}_p = RP \begin{bmatrix} 0 & \ell_2 & \ell_3 \\ 0 & -\ell_1 & 0 \\ 0 & 0 & -\ell_1 \end{bmatrix}. \tag{47}$$

The load stiffness matrix referred to the global coordinate system is obtained by using the standard coordinate transformation.

2.9. Equilibrium equations

The nonlinear equilibrium equations may be expressed by

$$\mathbf{\Psi} = \mathbf{F} - \lambda\mathbf{P} = \mathbf{0}, \tag{48}$$

where $\mathbf{\Psi}$ is the unbalanced force between the internal nodal force $\mathbf{F}$ and the external nodal force $\lambda\mathbf{P}$, where λ is the loading parameter, and $\mathbf{P}$ is a reference loading. Note that $\mathbf{P}$ may require to be updated at each iteration if the applied load is configuration dependent. $\mathbf{F}$ is assembled from the element nodal force

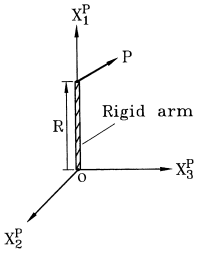

Fig. 3. Mechanism for generating configuration dependent moment by an off-axis load.

vectors, which are calculated using Eqs. (33)–(36) and (40) first in the current element coordinates and then transformed from current element coordinate system to global coordinate system before assemblage using standard procedure.

In this paper, a weighted Euclidean norm of the unbalanced force is employed as the error measure for the equilibrium iterations, and is given by

$$\frac{\|\mathbf{\Psi}\|}{|\lambda|\sqrt{N}} \leqslant e_{\text{tol}}, \tag{49}$$

where N is the number of equilibrium equations; e_{tol} is a prescribed value of error tolerance.

2.10. Criterion of the buckling state

Here, the zero value of the tangent stiffness matrix determinant is used as the criterion of the buckling state. The tangent stiffness matrix of the structure is assembled from the element stiffness matrix and load stiffness matrix. Let $\mathbf{K}_{\text{T}}(\lambda)$ denote the tangent stiffness matrix of the structure corresponding to the loading parameter λ. The criterion of the buckling state may be expressed as

$$D(\lambda) = \det|\mathbf{K}_{\text{T}}(\lambda)| = 0. \tag{50}$$

Let λ_{NB} denote the minimum loading parameter satisfying Eq. (50). λ_{NB} is called buckling loading parameter here.

The buckling mode corresponding to λ_{NB} may be obtained by solving the following generalized eigenvalue problem:

$$\mathbf{K}_0\mathbf{X} = -\frac{\lambda}{\lambda_{NB}}\mathbf{K}_G\mathbf{X}, \tag{51}$$

where $\mathbf{K}_0$ is the linear stiffness matrix of the structure, and $\mathbf{K}_G = \mathbf{K}_{\text{T}} - \mathbf{K}_0$ is the geometric stiffness matrix of the structure corresponding to λ_{NB}. It can be seen that λ_{NB} is also an eigenvalue for Eq. (51) The eigenvector corresponding to eigenvalue λ_{NB} is the required buckling mode. Here, the inverse power method [42] is used to find buckling mode.

3. Numerical algorithm

An incremental-iterative method based on the Newton–Raphson method combined with constant arc length of incremental displacement vector [21,43] is employed for the solution of nonlinear equilibrium equations. For a given displacement increment or corrector, the method described in [21,44] is employed to determine the current element cross-section coordinates, element coordinates and element deformation nodal parameters for each element. The parabolic interpolation method of the arc length proposed in [34] is employed here to find the buckling load. In order to initiate the secondary path, at the bifurcation point a perturbation displacement proportional to the first buckling mode is added [36].

4. Numerical studies

Example 1 (*Cantilever beam of angle section subjected to an end torque*). The example considered here is a cantilever beam of monosymmetric angle section with a pure torque T applied at its free end as shown in Fig. 4. This example was experimentally and theoretically studied by Gregory [1]. The clamped end of the beam is warping free. The geometry and material (brass) properties are: $L = 177.8$ mm, $\alpha = 90^\circ$, $b = 14.605$ mm, $t = 0.9601$ mm, Young's modulus $E = 89632$ MPa, the shear modulus $G = 33445$ MPa, and the specific weight $\gamma = 83.385$ N/cm^3.

The present results are obtained using 20 elements. Fig. 5 shows the path of point B in the centerline of the end cross-section obtained by the present study, the experimental results given in [1], and the

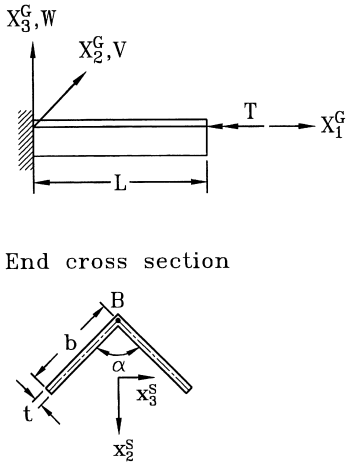

Fig. 4. Cantilever beam of angle section subjected to an end torque.

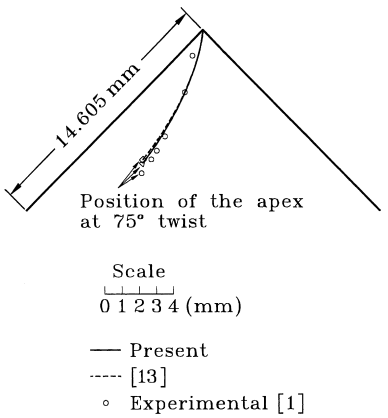

Fig. 5. Path of point B under end torque.

numerical results given in [13]. The material properties used in [13] are: $E = 89660$ MPa, and $G = 31130$ MPa. Very good agreement is observed between the present solutions and the experimental results.

Example 2 (*Cantilever beams subjected to an end force* (*buckling analysis*)). The elastic buckling loads of bisymmetric I-section, monosymmetric I-section and T-section cantilever beams subjected to a vertical downward end force P, as shown in Fig. 6 are studied here. This example was experimentally and theoretically investigated by Anderson and Trahair [5], and also studied by Attard [14] and by Pi and Trahair [22] using the finite element method. The clamped end of the beam is fully restrained against warping. The material properties, Young's modulus $E = 9445$ ksi and the shear modulus $G = 3766$ ksi used in [14] are employed here. The self-weight is not considered for this example. Four different section geometries are considered: (1) $b = 1.241$ in., $t_f = 0.1232$ in., $d = 2.975$ in., $t_w = 0.0862$ in. (bisymmetric I-section); (2) $b_1 = 1.241$ in., $t_1 = 0.1232$ in., $b_2 = 0.625$ in., $t_2 = 0.1231$ in., $d = 2.975$ in., $t_w = 0.0862$ in. (monosymmetric I-section); (3) $b_1 = 1.239$ in., $t_1 = 0.1236$ in., $b_2 = 1.238$ in., $t_2 = 0.0451$ in., $d = 2.897$ in., $t_w = 0.0863$ in. (monosymmetric I-section); (4) $b = 1.239$ in., $t_f = 0.1236$ in., $h = 2.8292$ in., $t_w = 0.0863$ in. (monosymmetric T-section). A total of 28 cases denoted by $NXxL$ are investigated, where $N = 1 - 4$, $X = A, B$, $x = a, b, c$, and $L = 65, 50$(in.). N means that section N is considered; A and B mean that the larger flange is at the bottom and at the top, respectively; the lower case letters a, b and c indicate the load

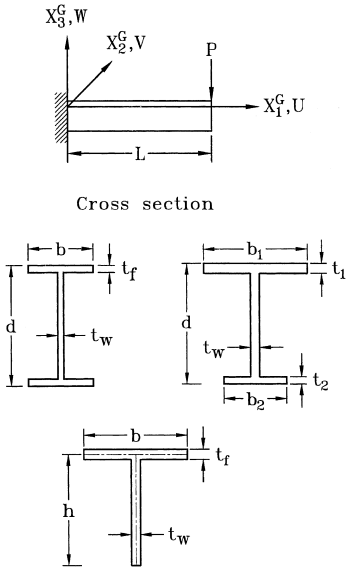

Fig. 6. Cantilever beams subjected to an end force (buckling analysis).

Table 1
Bucklingload for Example 2

Case	Bucklingload P_{NB} (lb)				
	Exp. [5]	Theory [5]	FEM [14]	FEM [22]	Present
1Aa65	59.7	56.8	–	56.5	56.2
1Ac65	72.7	74.2	–	76.1	74.5
1Aa50	91.2	94.6	–	92.1	91.8
1Ac50	134.2	139.2	–	141.8	138.1
2Aa65	37.8	36.5	36.6	36.0	37.0
2Ab65	57.4	57.7	58.9	56.9	58.0
2Ba65	32.8	31.3	31.7	32.7	31.8
2Bb65	37.7	38.7	39.1	37.5	39.0
2Aa50	56.8	58.0	57.5	56.8	58.6
2Ab50	105.3	110.3	112.6	109.6	111.2
2Ba50	51.0	52.1	51.9	50.7	52.4
2Bb50	64.8	66.7	67.9	66.0	67.7
3Aa65	35.6	36.6	–	35.7	36.8
3Ab65	59.1	61.6	–	61.3	61.9
3Ba65	38.3	35.8	–	36.8	35.8
3Bb65	47.8	49.4	–	48.9	49.3
3Aa50	61.6	58.4	–	59.6	58.2
3Ab50	111.6	118.9	–	118.7	121.0
3Ba50	61.0	58.4	–	57.7	59.7
3Bb50	90.2	91.8	–	90.4	92.1
4Aa65	29.2	26.7	26.7	28.0	27.3
4Ab65	43.0	42.6	45.2	46.3	45.0
4Ba65	21.2	21.4	21.1	21.6	21.9
4Bb65	22.9	24.6	24.5	23.0	25.3
4Aa50	45.4	40.9	40.2	42.7	41.6
4Ab50	84.2	79.4	84.3	89.0	84.3
4Ba50	33.6	32.7	32.1	33.2	33.7
4Bb50	37.8	38.2	37.1	38.0	39.4

acts at the upper face, the lower face, and the centroid, respectively; L indicates the lengths of the beam. The present buckling loads obtained using five elements are shown in Table 1 together with those given in [5,14,22]. It can be seen that the agreement between all results is very good.

Example 3 (*Cantilever beam of channel section subjected to an end force*). This example considered here is a cantilever beam of monosymmetric channel section with a vertical end force P applied at the top of the web as shown in Fig. 7. The example was first analyzed by Gruttmann et al. [29]. The clamped end of the beam is fully restrained against warping. The geometry and material properties are as follows: $L = 900$ cm, $b = 10$ cm, $t_f = 1.6$ cm, $h = 28.4$ cm, $t_w = 1.0$ cm, Young's modulus $E = 21000$ kN/cm^2, and Poisson's ratio $v = 0.3$.

The present results are obtained using 30 elements. The load–deflection curves of the present study together with the two results given in [29], which were obtained using 20 two-node beam elements and 180 four-node shell elements, respectively, are shown in Figs. 8 and 9. As can be seen that the agreement is very good between the present results and the results of [29] obtained by using the shell element. Note that even a fairly sharp break appears in each deflection curve, in this study no buckling load is found for this example. Note that no buckling load was reported in [29] also for this example.

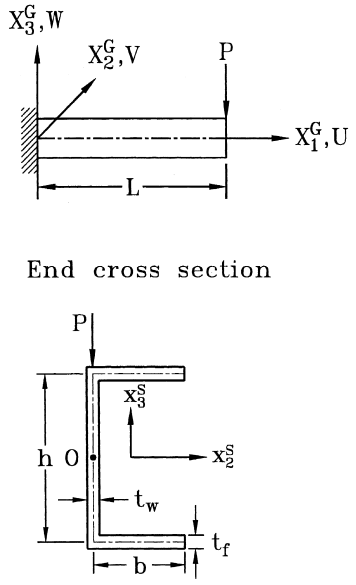

Fig. 7. Cantilever beam of channel section subjected to an end force.

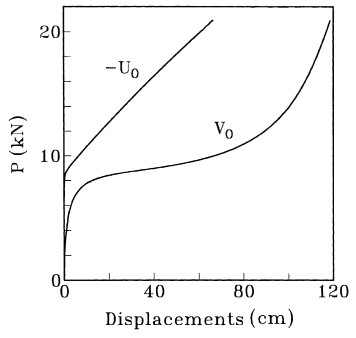

Fig. 8. Load–tip displacements (U, V) for cantilever beam of Example 3.

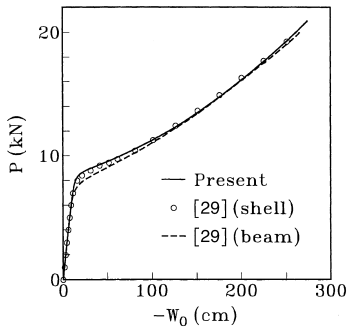

Fig. 9. Load–tip displacements (W) for cantilever beam of Example 3.

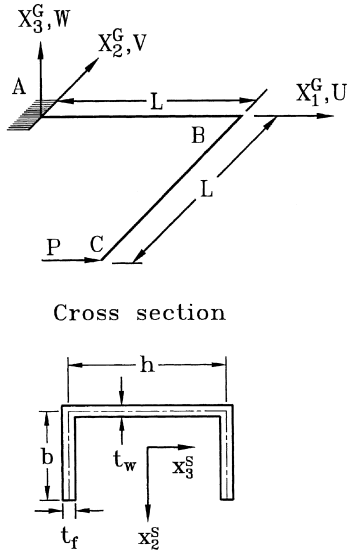

Fig. 10. Cantilever right-angle frame subjected to an end force.

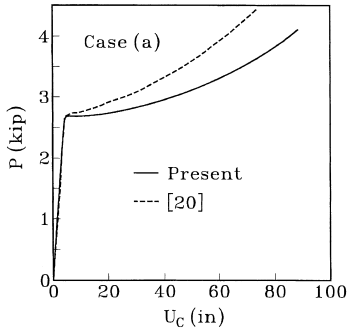

Fig. 11. Load–displacement (U) curves for case (a) of Example 4.

Example 4 (*Cantilever right-angle frame of channel section subjected to an end force*). The example considered is a cantilever right-angle frame with an in-plane force P applied at the shear center of the end cross-section as shown in Fig. 10. This example was analyzed by Chen and Blandford [20]. Each member of the frame has a C15 × 50 section with the web lying in the plane of the frame. The geometry and material properties are as follows: $L = 240$ in., $b = 3.716$ in., $t_f = 0.65$ in., $h = 15$ in., $t_w = 0.716$ in., Young's

modulus $E = 29000$ ksi, and the shear modulus $G = 11200$ ksi. Here, two cases are considered for the warping condition at member ends: (a) Warping free at the fixed end, corner joint connecting two members, and free end, and (b) Warping restrained at the fixed end and corner joint, and warping free at free end.

The frame is analyzed using 8, 40 and 80 elements. The load–deflection curves of the present study obtained using 80 elements together with the results obtained by Chen and Blandford [20] using eight updated Lagrangian beam elements are shown in Figs. 11–13, for case (a) and Figs. 14–16 for case (b). The present results obtained using 40 and 80 elements are nearly identical. The agreement between the results of the present study obtained using eight element (not shown) and those of [20] obtained using eight elements is fairly good. As can be seen that the results of the present study and [20] are nearly identical when the load is less than 2.69 kip for case (a) and 3.00 kip for case (b). However, their discrepancy is not negligible as the load approximately exceeds 2.75 kip for case (a) and 3.10 kip for case (b). It was reported in [20] that the

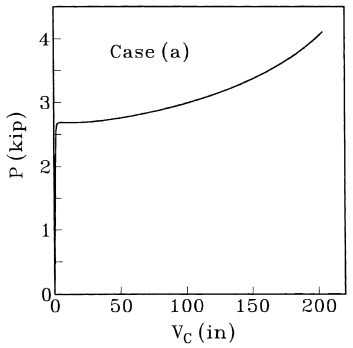

Fig. 12. Load–displacement (V) curve for case (a) of Example 4.

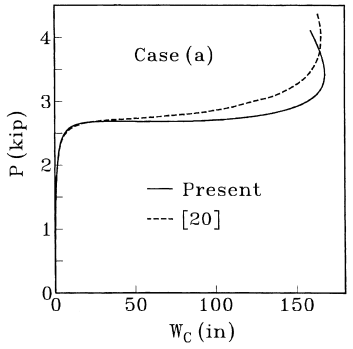

Fig. 13. Load–displacement (W) curves for case (a) of Example 4.

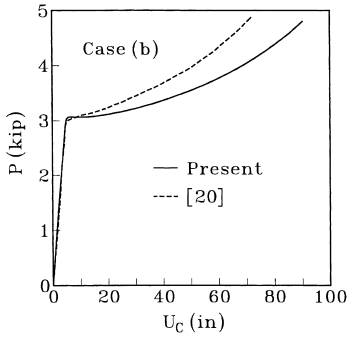

Fig. 14. Load–displacement (U) curves for case (b) of Example 4.

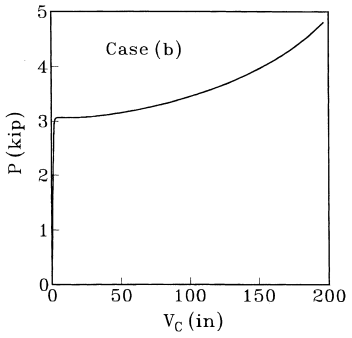

Fig. 15. Load–displacement (V) curves for case (b) of Example 4.

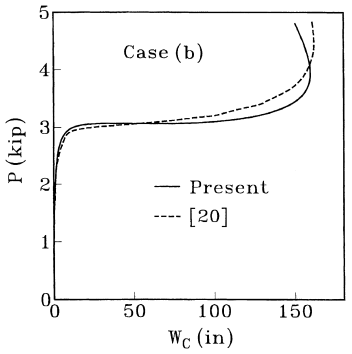

Fig. 16. Load–displacement (W) curve for case (b) of Example 4.

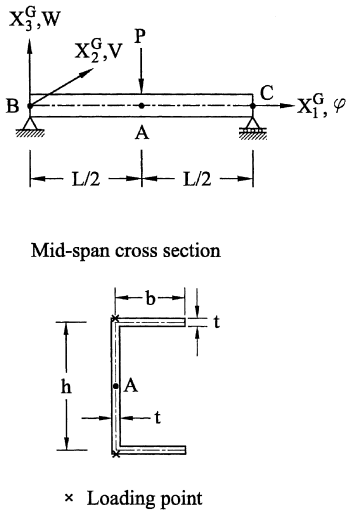

Fig. 17. Simply supported beam of channel section subjected to a mid-span force.

buckling loads were 2.488 kip and 2.939 kip for cases (a) and (b), respectively. However, in this study no buckling load is found for both cases.

Example 5 (*Simply supported beam of channel section subjected to a mid-span force*). The example considered is a simply supported beam of channel section subjected to a mid-span concentrated load P, as shown in Fig. 17. The ends of the beam are free to warp and free to rotate about X_2^G and X_3^G axes, but

restrained from rotation about X_1^G axis. The translation is restrained at end point B, and is free only in the direction of X_1^G axis at points C. The geometrical and material properties are $b = 16$ cm, $t_f = t_w = t = 1.6$ cm , $h = 40$ cm, $L/h = 15$, 30 and 45, Young's modulus $E = 20600$ N/cm^2 and Poisson's ratio $v = 0.3$. Two different loading points (see Fig. 17), top flange (TF) and bottom flange (BF), are considered.

The present results are obtained using 40 elements. No buckling load is found for each case The load–deflection curves are shown in Figs. 18–20. As can be seen that the span length and the location of loading point are important factors for the load carrying capacity of this example.

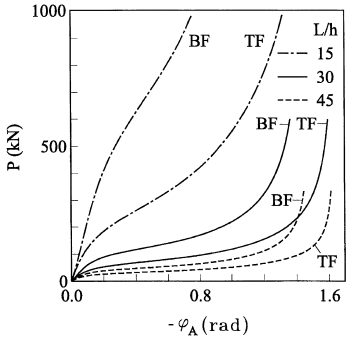

Fig. 18. Load–twist angle curves for Example 5.

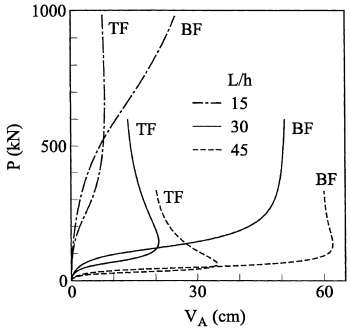

Fig. 19. Load–displacement (V) curves for Example 5.

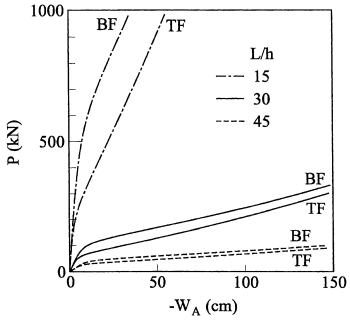

Fig. 20. Load–displacement (W) curves for Example 5.

5. Conclusions

This paper has proposed a consistent co-rotational total Lagrangian finite element formulation for the geometric nonlinear buckling and postbuckling analysis of monosymmetric thin-walled beams with open section. All coupling among bending, twisting, and stretching deformations for beam element is considered by consistent second-order linearization of the fully geometrically nonlinear beam theory. The third-order term of the twist rate of the beam axis is also considered in element nodal forces. An incremental-iterative method based on the Newton–Raphson method combined with constant arc length of incremental displacement vector is employed for the solution of nonlinear equilibrium equations. The zero value of the tangent stiffness matrix determinant of the structure is used as the criterion of the buckling state. From the numerical examples studied, it is found that the agreement between the prebuckling displacements and buckling loads of the present study and those given in the literature is very good. However, differences between the postbuckling deflections of the present study and those given in the literature become significant for some cases.

References

[1] M. Gregory, A nonlinear bending effect when certain unsymmetical sections are subjected to a pure torque, Austral. J. Appl. Sci. 11 (1960) 33–48.
[2] V.Z. Vlasov, Thin Walled Elastic Beams, second ed., 1961 (English translation published for U.S. Science Foundation by Israel Program for Scientific Translations).
[3] S.P. Timoshenko and J.M. Gere, Theory of Elastic Stability, second ed., McGraw-Hill, New York, 1963.
[4] R.S. Barsoum, R.H. Gallagher, Finite element analysis of torsional and torsional-flexural stability problems, moments,, Internat. J. Numer. Methods Engrg. 2 (1970) 335–352.
[5] J.M. Anderson, N.S. Trahair, Stability of monosymmetric beams and cantilevers, J. Struct. Div. ASCE 98 (1972) 269–286.
[6] S.T. Woolcock, N.S. Trahair, Post-buckling behavior of determinate beams, J. Engrg. Mech. Div. ASCE 100 (1974) 151–171.
[7] D.O. Brush, B.O. Almroth, Buckling of Bars, Plates and Shells, McGraw-Hill, NewYork, 1975.
[8] H. Ziegler, Principles of Structural Stability, Birkhauser, Basel, 1977.
[9] J.H Argyris, P.C. Dunne, D.W. Scharpf, On large displacement-small strain analysis of structures with rotation degree of freedom, Comput. Methods Appl. Mech. Engrg. 14 (1978) 401–451.
[10] J.H Argyris, P.C. Dunne, D.W. Scharpf, On large displacement-small strain analysis of structures with rotation degree of freedom, Comput. Methods Appl. Mech. Engrg. 15 (1978) 99–135.
[11] J.H. Argyris, O. Hilpert, G.A. Malejannakis, D.W. Scharpf, On the geometrical stiffness of a beam in space – a consistent v.w. approach, Comput. Methods Appl. Mech. Engrg. 20 (1979) 105–131.
[12] J.H. Argyris, H. Balmer, J.St. Doltsinis, P.C. Dunne, M. Haase, M. Kleiber, G.A. Malejannakis, H.P. Mlejenek, M. Muller, D.W. Scharpf, Finite element method – the natural approach, Comput. Methods Appl. Mech. Engrg. 17/18 (1979) 1–106.
[13] M.M. Attard, The elastic flexural-torsional response of thin-walled open beams, Ph.D. Thesis, University of New South Wales, Australia, 1984.
[14] M.M. Attard, Lateral buckling analysis of beams by FEM, Comput. and Struct. 23 (1986) 217–231.
[15] J.C. Simo, L. Vu-Quoc, A three-dimensional finite strain rod model. Part II: Computational aspects, Comput. Methods Appl. Mech. Engrg. 58 (1986) 79–116.
[16] W.F. Chen, E.M. Lui, Structural Stability, Theory and Implementation, Elsevier, New York, 1988.
[17] A. Cardona, M. Geradin, A beam finite element non-linear theory with finite rotations, Internat. J. Numer. Methods Engrg. 26 (1988) 2403–2438.
[18] M. Iura, S.N. Atluri, On a consistent theory and variational formulation of finitely stretched and rotated 3-D spaced-curved beams, Comput. Mech. 4 (1989) 73–88.
[19] M.A. Crisfield, A consistent co-rotational formulation for non-linear three-dimensional beam elements, Comput. Methods Appl. Mech. Engrg. 81 (1990) 131–150.
[20] H. Chen, G.E. Blandford, Thin-walled space frames, part I: large deformation analysis theory, and part II: algorithmic details and applications, J. Struct. Engrg. ASCE 117 (1991) 2499–2539.
[21] K.M. Hsiao, Corotational total Lagrangian formulation for three-dimensional beam element, AIAA J. 30 (1992) 797–804.
[22] Y.L. Pi, N.S. Trahair, Prebuckling deflections and lateral buckling: part I: theory and part II: application, J. Struct. Engrg. ASCE 118 (1992) 2949–2985.
[23] A.S. Gendy, A.F. Saleeb, Generalized mixed finite element model for pre-and post-quasistatic buckling response of thin-walled framed structures, Internat. J. Numer. Methods Engrg. 37 (1994) 297–322.
[24] B.A. Izzuddin, An Eulerian approach to the large displacement analysis of thin-walled frames, Proc. Inst. Civil Engrs. Structs. and Bldgs. 110 (1995) 50–65.
[25] G. Jelenic, M. Saje, A kinematically exact space finite strain beam model-finite element formulation by generalized virtual work principle, Comput. Methods Appl. Mech. Engrg. 120 (1995) 131–161.

[26] B.A. Izzuddin, D.L. Smith, Large-displacement analysis of elastoplastic thin-walled frames. Part I: formulation and implementation and part II: verification and application, J. Struct. Engrg. ASCE 122 (1996) 905–925.
[27] K.M. Hsiao, R.T. Yang, W.Y. Lin, A consistent finite element formulation for linear buckling analysis of spatial beams, Comput. Methods Appl. Mech. Engrg. 156 (1998) 259–276.
[28] L.H. Teh, M.J. Clarke, Co-rotational and Lagrangian formulations for elastic three-dimensional beam finite elements, J. Construct. Steel Res. 48 (1998) 123–144.
[29] F. Gruttmann, R. Sauer, W. Wagner, A geometrical nonlinear eccentric 3D-beam element with arbitrary cross-sections, Comput. Methods Appl. Mech. Engrg. 160 (1998) 383–400.
[30] K.M. Hsiao, W.Y. Lin, A co-rotational finite element formulation for buckling and postbuckling analysis of spatial beams, Comput. Methods Appl. Mech. Engrg. 188 (2000) 567–594.
[31] K. Mattiasson, A. Samuelsson, Total and updated Lagrangian forms of the co-rotational finite element formulation in geometrically and materially nonlinear analysis, in: C. Tailor, E. Hinton, D.R.J. Owen (Eds.), Numerical Methods for Non-linear Problems, vol. 2, Pineridge, Swansea, 1984, pp. 135–151.
[32] J.C. Simo, L. Vu-Quoc, The role of non-linear theories in transient dynamic analysis of flexible structures, J. Sound Vib. 119 (1987) 487–508.
[33] R.D. Cook, W.C. Young, Advanced Mechanics of Materials, Macmillan, New York, 1985.
[34] K.M. Hsiao, W.Y. Lin, A co-rotational finite element formulation for buckling and postbuckling analysis of doubly symmetric thin-walled beams, Comput. Methods Appl. Mech. Engrg., submitted.
[35] S. Timoshenko, Strength of Materials. Prat II: Advanced Theory and Problems, Van Nostrand, Princeton, NJ, 1956.
[36] T. Matsui, O. Matsuoka, A new finite element scheme for instability analysis of thin shells, Internat. J. Numer. Methods Engrg. 10 (1976) 145–170.
[37] H. Goldstein, Classical Mechanics, Addision-Wesley, Reading, MA, 1980.
[38] T.J. Chung, Continuum Mechanics, Prentice-Hall, Englewood Cliffs, NJ, 1988.
[39] D.J. Dawe, Matrix and Finite Element Displacement Analysis of Structures, Oxford University Press, New York, 1984.
[40] L.H Teh, M.J. Clarke, Symmetry of tangent stiffness matrices of 3D elastic frame, J. Engrg. Mech. ASCE 125 (1999) 248–251.
[41] K.S. Schweizerhof, E. Ramm, Displacement dependent pressure loads in nonlinear finite element analysis, Comput. and Struct. 18 (1984) 1099–1114.
[42] K.J. Bathe, Finite Element Procedure in Engineering Analysis, Prentice-Hall, Englewood Cliffs, NJ, 1982.
[43] M.A. Crisfield, A fast incremental/iterative solution procedure that handles snap through, Comput. and Struct. 13 (1981) 55–62.
[44] K.M. Hsiao, C.M. Tsay, A motion process for large displacement analysis of spatial frames, Internat. J. Space Struct. 6 (1991) 133–139.